Journal of the European Ceramic Society **14** (1994) 111–116

In-situ Scanning Acoustic Microscopy of Crack Bridging in Alumina

T. J. Marrow, G. A. D. Briggs & S. G. Roberts

Department of Materials, Oxford University, Parks Road, Oxford OX1 3PH, UK

(Received 18 November 1993; revised version received 24 February 1994; accepted 8 March 1994)

Abstract

High-resolution scanning acoustic microscopy has been used to observe crack bridging in a fine-grained polycrystalline alumina. The microscope is sensitive to the increased acoustic transmission across the crack from the interlocking and sliding asperities that cause crack shielding and R-curve behaviour. Acoustic microscopy is found to be more reliable than optical microscopy for characterising crack bridging. The bridging zone size, bridge density and bridge failure strain are easily determined. The technique may be of considerable use in characterising R-curve mechanisms in a wide range of microstructures.

Rißbrücken in feinkörnigem, polykristallinem Aluminiumoxyd wurden mit Hilfe der Rasterakustomikroskopie untersucht. Aufgrund der erhöhten akustischen Transmission an den Rißkontaktstellen, die für die Rißabschirmung und das R-Kurvenverhalten verantwortlich sind, lassen sich diese im Mikroskop sichtbar machen. Es hat sich gezeigt, daß das Akustomikroskop zur Untersuchung der Rißbrücken besser geeignet ist als das Lichtmikroskop. Die Größe der Brückenzonen, die Brückendichte und die Dehnung beim Versagen der Brücken lassen sich in einfacher Weise bestimmen. Die Methode kann für die Charakteriserung des R-Kurvenmechanismuses für verschiedenste Gefüge von Interesse sein.

Le microscope acoustique à haute résolution a été utilisé pour observer le pontage des fissures dans une alumine polycristalline à grains fins. Le microscope est sensible à l'augmentation de la transmission acoustique à travers la fissure à cause de l'interconnection et du glissement des aspérités qui causent un écrantage des fissures et un comportement de type courbe R. Le microscope acoustique est donc beaucoup plus fiable que le microscope optique lorsqu'il s'agit de caractériser les pontages de fissures. La zone de pontage, la densité du pontage et les contraintes d'un défaut de pontage sont aisément déterminables. Cette technique peut être d'une aide considérable pour l'interprétation des courbes R d'un grand nombre de microstructures.

1 Introduction

The *R*-curve behaviour observed in many engineering ceramics, particularly alumina,[1,2] i.e. rising fracture toughness with increasing crack length, is of great importance to their successful use in load-bearing applications. A strong *R*-curve induces flaw tolerance,[3] which stabilises cracks and reduces the variation in fracture strength of ceramic components.[4] From studies of polycrystalline alumina, the general mechanisms of *R*-curve generation are understood. However, a fully quantitative model for the effects of microstructure has yet to be developed.

The room-temperature *R*-curve of fine to medium grain size alumina (typically less than around 30 μm) depends on crack-wake processes[5] and increases in magnitude with increasing grain size.[6] The behaviour arises from crack–face interactions, with no evidence of a microcrack process zone. Crack bridging, by non-fractured grains,[7] interlocking grains[8] and friction of asperities[6–8] causes traction in the crack wake, shielding the crack tip from the applied stress. The maximum length of the bridging zone depends on the crack opening displacement[9] and therefore increases with increasing grain size.[6] Since the crack profile is influenced by crack bridging,[8] the bridging zone size and the *R*-curve are both material and specimen dependent.[9,10]

Careful in-situ observations of bridged cracks using optical and scanning electron microscopy indicate that bridging zones can extend over a few

Journal of the European Ceramic Society 0955-2219/94/$7.00

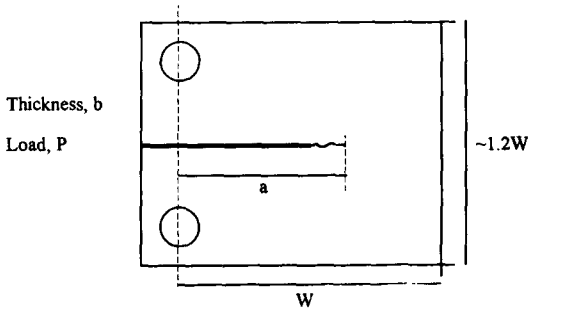

Notch Width 300μm a = 11mm W = 20.5mm b = 2.8mm

$$K = \frac{P}{b\sqrt{W}} \frac{(2+\alpha)}{(1-\alpha)^{3/2}} (0.886 + 4.64\alpha - 13.32\alpha^2 + 14.72\alpha^3 - 5.6\alpha^4) \qquad \alpha = a/W$$

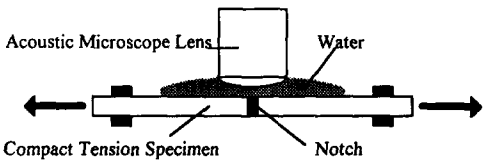

Lens - specimen separation approximately 20μm.

Fig. 1. Compact tension specimen dimensions and experimental arrangement for in-situ observations (not to scale).

hundred[11] to several thousand grain diameters,[6] depending on the specimen geometry and thus the crack opening profile. The fracture surface coverage (density) of bridges has been estimated at from 10%[6] up to around 25%.[11,12] Tensile tests of the unfractured crack bridging zone predict a bridge density of 14%.[13]

Simple models for bridge formation and fracture[6] suggest that only frictional interlocking and subsequent pull-out of grains are sufficient to account for the observed *R*-curves and bridging zone lengths. The gradual decrease in average bridging stress with increasing crack opening, predicted by grain pull-out models, has been confirmed by tensile tests of bridging zones.[14] Frictional wear of asperities has also been observed,[6,8] and cyclic loading, and thus the abrasion of asperities, decreases the *R*-curve.[15]

A number of models based on the grain pull-out mechanism have been developed to predict the *R*-curve behaviour for both long and short crack specimen geometries.[7,10,12,16,17] Reasonable agreement has been found with observed bridge distributions and *R*-curves. However, other than macroscopic measurements of the average post-fracture bridging zone tensile strength,[13,14] there are no direct microscopic observations of the relationship between crack opening and individual bridge strength.

High-resolution scanning acoustic microscopy has been used to demonstrate crack bridging in alumina following high-temperature slow crack growth[18] and room-temperature slow crack growth.[19] The in-situ experiment described in this paper was performed to determine whether scanning acoustic microscopy is a suitable technique for characterising the strength and distribution of crack bridging in a fine-grained alumina.

2 Experimental details

A high purity alumina, supplied by Dynamic Ceramic Ltd, (Stoke-on-Trent, UK) was used. The microstructure consisted of equiaxed grains with a mean size of 3·7 μm ± 1·7 μm (determined using the line intercept method). A compact tension specimen (Fig. 1) was prepared using a high-speed diamond-tipped drill and saw. One surface was then polished, finishing with 1 μm diamond paste.

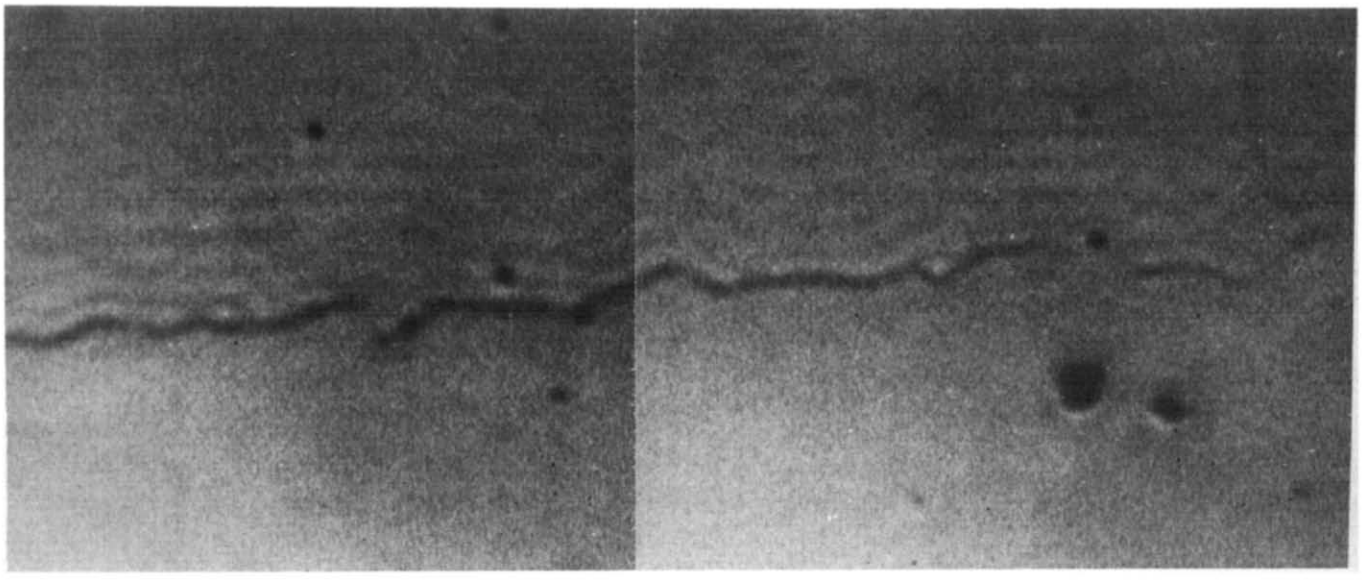

Fig. 2. Crack tip loaded to 2MPa√m. Imaged at 1·6GHz, defocused by −1 μm.

The pre-crack was initiated by a 15 kg Vickers indentation at the notch tip. The specimen was waxed to a glass plate during the indentation, and was then immersed in water after indentation to promote stable crack growth. The crack extended approximately 1·5 mm from the notch tip. The radial crack length from a 15 kg indentation placed at some distance from the notch tip was less than 200 μm.

The in-situ experiment was performed using a 500N straining stage mounted on a Leitz ELSAM scanning acoustic microscope, operating at 1·6–1·7GHz, using water at 60°C as the coupling medium, giving a resolution of approximately 0·9 μm. The straining stage was designed and constructed by the National Physical Laboratory[20] and was adapted for use with the compact tension specimen for this experiment. The experimental arrangement for the in-situ observations is shown in Fig. 1.

The crack was observed using the scanning acoustic microscope both unloaded and at stress intensities of 0·8MPa$\sqrt{m}$ and 2MPa$\sqrt{m}$. The applied stress intensity, K, was calculated from the applied load using the standard expression, given in Fig. 1. Optical microscopy was also used for comparison with the acoustic microscopy, with Nomarski interferometry for enhanced contrast. The specimen failed by rapid crack growth and fracture shortly after the crack was loaded to 2·5MPa$\sqrt{m}$. The fracture surface was gold-sputtered and examined using scanning electron microscopy (SEM).

3 Results

The crack was difficult to image without an applied load by either optical or scanning acoustic microscopy (SAM), except for the region close to the indentation where residual stresses held the crack open. A stress intensity of 0·8MPa$\sqrt{m}$ was sufficient to open the crack and increased the SAM image contrast. The crack tip region was then clearly visible using SAM (Fig. 2). However, the crack tip position determined by optical microscopy was 50 μm short of that determined using SAM. The crack tip position determined by SAM was shown to be the true crack tip by inspection of the fracture surface and crack profile in the SEM. SEM also confirmed that the crack was straight and uniform across the specimen thickness. The fracture surface showed mixed intergranular and transgranular fracture modes. The crack tip stress intensity contribution from the residual stress field of the indentation was assumed to be negligible due to the order of magnitude difference between the equilibrium indentation crack and that produced by the wedging effect of the indentor at the notch tip.

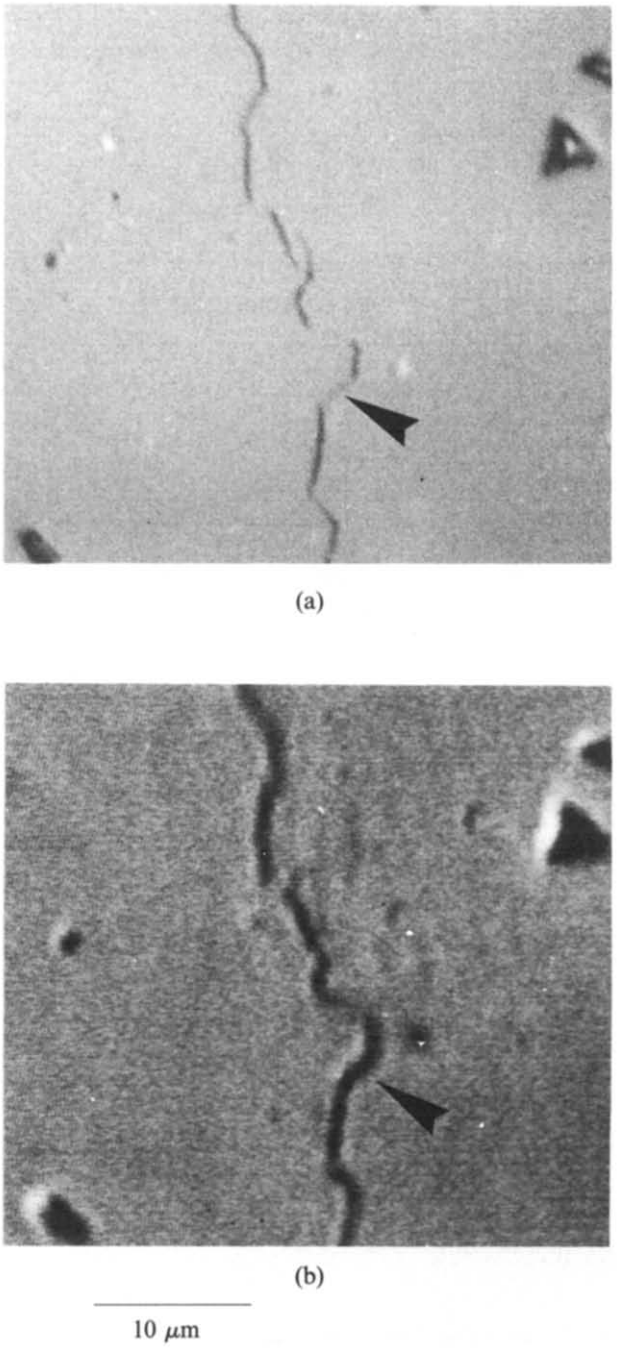

Fig. 3. A group of crack bridges observed using (a) optical microscopy and (b) scanning acoustic microscopy (1·7GHz, defocused by −1·5 μm). The large bridge (arrowed) indicated by optical microscopy is not observed using scanning acoustic microscopy.

Isolated regions of zero or low contrast, smaller than 5 μm, were observed using both SAM and optical microscopy (Figs 2 and 3). These were identified as crack bridges. The crack bridge distributions, determined using SAM and optical microscopy with the crack loaded to 2MPa$\sqrt{m}$, are compared in Fig. 4. Distances were measured from the crack tip position determined by SAM. Fewer bridges were observed using SAM, and many bridges indicated by optical microscopy

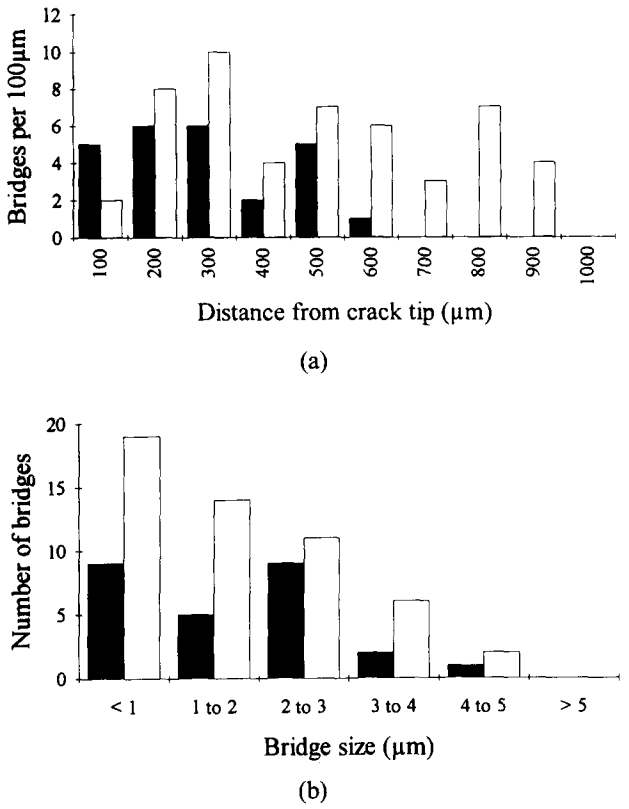

Fig. 4. (a) The distribution of crack bridges with distance from the crack tip, determined using (□) optical and (■) scanning acoustic microscopy. The crack tip position was measured using scanning acoustic microscopy. (b) The distribution of crack bridge size observed using (□) optical and (■) scanning acoustic microscopy.

were not observed using SAM (Fig. 3). The maximum bridging zone size determined using SAM (600 μm) was significantly smaller than that indicated by optical microscopy (900 μm) (Fig. 4(a)). Some bridges which were observed using SAM at 0·8MPa$\sqrt{m}$ disappeared when the stress intensity was increased to 2MPa$\sqrt{m}$ (Fig. 5). There was no evidence of extensive microcracking in the crack wake or ahead of the crack tip.

4 Discussion

The marked increase in contrast on opening the crack demonstrates that the SAM image is sensitive to crack closure. The loss of image contrast with closure is due to Rayleigh wave transmission across the crack.[18,21] Theoretically, using Rayleigh wave reflection, SAM is capable of imaging planar cracks opened wider than a few nanometres,[22] but transmission due to surface roughness contact reduces this contrast and decreases the resolution. Nevertheless, SAM is very sensitive to open cracks. Crack bridges, where interlocking and frictionally sliding asperities increased transmission, were therefore indicated by localised regions of low or zero contrast (Figs 2 and 3). The image in the optical microscope was sensitive to the crack opening, and using Normarski interferometry, relative shear displacements of material on either size of the crack could be seen. Open cracks were dark and non-reflective and low contrast indicated that the crack faces were very close or touching. Crack–face tractions may have reduced shear displacements in the crack plane, further decreasing the Nomarski image contrast.

In comparison with optical microscopy, SAM indicated a smaller number of bridges and a reduced bridging zone size (Fig. 4(a)). This cannot have arisen simply from the lower spatial resolution of SAM, although this did obscure a significant fraction of sub-micron bridges (Fig. 4(b)). The anomalous low number of bridges detected by optical microscopy within 100 μm of the crack

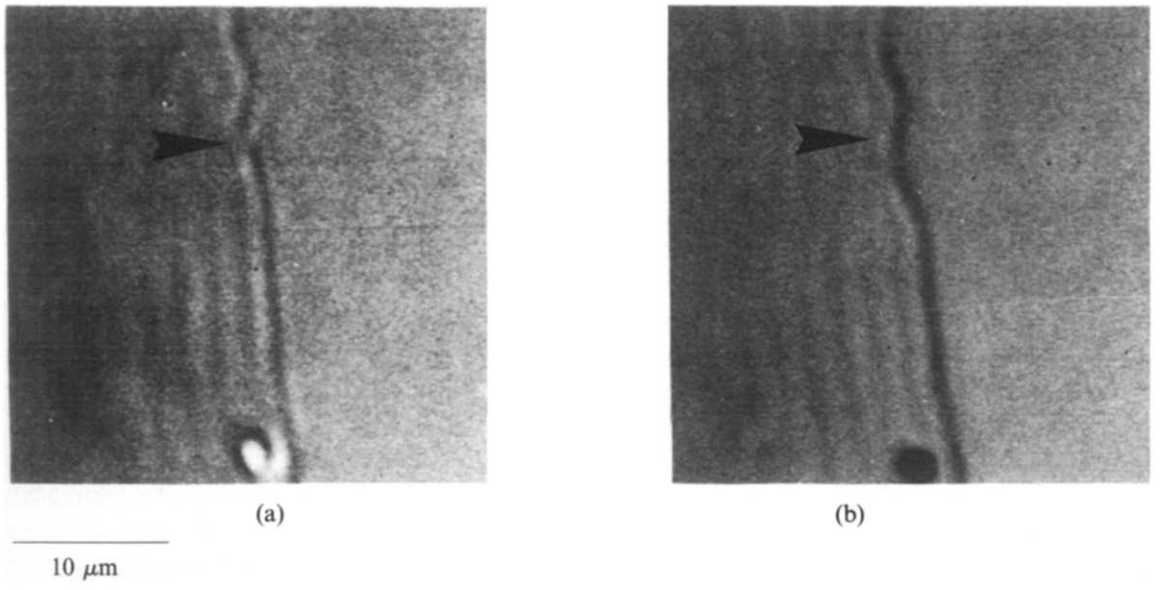

Fig. 5. The crack imaged using scanning acoustic microscopy at 1·6GHz, defocused by −1·5 μm at (a) 0·8MPa$\sqrt{m}$ and (b) 2MPa$\sqrt{m}$. The crack bridge, marked (1), disappears as the load and the crack opening displacement increase.

tip (Fig. 4(a)) was an artefact of the poor visibility of the 50 μm region nearest to the crack tip. Regions identified as large bridges using optical microscopy frequently showed strong contrast when imaged using SAM (Fig. 3), indicating that there was in fact no contact between the crack faces at this point. The majority of bridges (60%) observed by SAM corresponded to bridges detected using optical microscopy.

The Rayleigh waves which generated the SAM image penetrated approximately one wavelength (3·5 μm at 1·6GHz) below the surface. The SAM image therefore represented a surface layer of single grain thickness. Bridges indicated in the optical microscope, but which were not observed in the SAM, may have been due to true bridges below this layer reducing the crack opening. Crack contrast in the optical microscope may also have been reduced by reflections from inclined crack faces. Cracks which were not widely open may also have had low contrast. The SAM observations are therefore considered to be more representative of the true distribution of crack bridges.

The SAM observations indicated that the average density of bridging grains was approximately 5 grains per 100 μm. For an average grain size of 3·7 μm the bridge density was approximately 20%, which is comparable to previous estimates.[6,11,13] The crack opening displacement was measured, using optical microscopy, at the maximum extent of the bridging zone observed in the SAM to be approximately 0·45 μm. The bridge failure displacement was therefore approximately 12% of the mean grain size. This agrees with previous SEM observations which yielded failure strains of between 5% and 10% (determined from figures in Ref. 8[12]) and 12%.[13]

Scanning acoustic microscopy is therefore capable of detecting the crack–surface interactions associated with crack bridging, and is generally a more discriminating technique than optical microscopy. The bridging zone characteristics determined by SAM are comparable to independent measurements in the literature. SAM can be used for in-situ observations of bridge failure (Fig. 5), and it may be possible to observe stable crack growth and bridge formation using a more suitable specimen design. Future experiments will be performed using a coarser grain size alumina, ideally around 20 μm, to increase the average bridge size and allow clearer observations of the SAM signal at bridges. Quantitative observations will then determine the variation of bridge density with crack opening displacement. This may provide a link between the theoretical grain pull-out model[16] and tensile strength measurements of the crack bridging zone.[13,14]

5 Conclusions

Crack bridging in fine-grained polycrystalline alumina can be observed using high-resolution scanning acoustic microscopy. The microscope detected the increased transmission of acoustic waves across the crack at crack bridges, which were formed by interlocking grains and frictional contact of asperities. The size, distribution and failure strain of crack bridges was measured. Further quantitative work will continue with coarser microstructures. High-resolution scanning acoustic microscopy may be of considerable use for observing toughening mechanisms in other materials which show strong *R*-curves, such as ceramic matrix composites and transformation-toughened ceramics.

Acknowledgements

The authors would like to thank Professor R. J. Brook for provision of laboratory facilities. The research was funded by SERC Grant No. GR G 42853.

References

1. Chantikul, P., Bennison, S. J. & Lawn, B. R. Role of grain size in the strength and *R*-curve properties of alumina. *J. Am. Ceram. Soc.*, **73** (1990) 2419–27.
2. Steinbrech, R. W., Toughening mechanisms in ceramic materials. *J. Eur. Ceram. Soc.*, **10** (1992) 131–42.
3. Bennison, S. J. & Lawn B. R., Flaw tolerance in ceramics with rising crack resistance characteristics. *J. Mater. Sci.*, **24** (1989) 3169–75.
4. Cook, R. F. & Clarke, D. R., Fracture stability, *R*-curves and strength variability. *Acta Metall.*, **36** (1988) 555–62.
5. Knehans, R. & Steinbrech, R. W., Memory effect of crack resistance during slow crack growth in notched alumina bend specimens. *J. Mater. Sci. Lett.*, **1** (1982) 327–9.
6. Vekinis, G., Ashby, M. F. & Beaumont, P. W. R., *R*-curve behaviour of alumina ceramics. *Acta Metall.*, **38** (1990) 1151–62.
7. Cook. R. F., Segregation effects in the fracture of brittle materials: Ca–Al_2O_3. *Acta Metall.*, **38** (1990) 1083–100.
8. Rödel, J., Kelly, J. F. & Lawn, B. R., In-situ measurements of bridged crack interfaces in the scanning electron microscope. *J. Am. Ceram. Soc.*, **73**, (1990) 3313–18.
9. Steinbrech, R. W., Deuerler, F., Reichl, A. & Schaarwächter, W., Correlation of crack opening displacement and crack resistance curve of alumina. *Sci. Ceram.*, **14** (1988) 659–64.
10. Steinbrech, R. W., Reichl, A. & Schaarwächter, W., *R*-curve behaviour of long cracks in alumina. *J. Am. Ceram. Soc.*, **73** (1990) 2009–15.
11. Swanson, P. L., Fairbanks, C. J., Lawn, B. R., Mai, Y. W. & Hockey, B. J., Crack–interface grain bridging as a fracture resistance mechanism in ceramics, I: experimental study on alumina. *J. Am. Ceram. Soc.*, **70** (1987) 279–89.
12. Bennison, S. J. & Lawn, B. R., Role of interfacial grain-bridging sliding friction in the crack resistance and strength properties of non-transforming ceramics. *Acta Metall.*, **37** (1989) 2659–71.

13. Reichl, A. & Steinbrech, R. W., Determination of crack bridging forces in alumina. *J. Am. Ceram. Soc.*, **71**, (1988) C299–C300.
14. Hay, J. C. & White, K. W., Grain bridging mechanisms in monolithic alumina and spinel. *J. Am. Ceram. Soc.*, **76** (1993) 1849–54.
15. Hu, X. & Mai, Y. W., Crack bridging analysis for alumina ceramics under monotonic and cyclic loading. *J. Am. Ceram. Soc.*, **75** (1992) 848–53.
16. Mai, Y. W. & Lawn, B. R., Crack–interface grain bridging as a fracture resistance mechanism in ceramics, II: theoretical fracture mechanics model. *J. Am Ceram. Soc.*, **70** (1987) 289–94.
17. Llorca, J. & Steinbrech, R. W., Fracture of alumina: an experimental and numerical study. *J. Mater. Sci.*, **26** (1991) 6383–90.
18. Marrow, T. J., Luprano, V. & Roberts, S. G., Scanning acoustic microscope observations of high temperature crack bridging mechanisms in alumina. *J. Am. Ceram. Soc.*, **76** (1993) 2915–18.
19. Quinten, A. & Arnold, W., Observations of stable crack growth in Al_2O_3 ceramics using a scanning acoustic microscope. *Mater. Sci. Eng.*, **A122** (1989) 15–19.
20. Weaver, J. M. R. PhD Thesis, University of Oxford, 1987.
21. Somekh, M. G., Bertoni, H. L., Briggs, G. A. D. & Burton, N. J., A two-dimensional imaging theory of surface discontinuities with the scanning acoustic microscope. *Proc. Roy. Soc Lond.*, **A401**, (1985) 29–51.
22. Briggs, G. A. D., Acoustic microscopy. In *Monographs on the Physics and Chemistry of Materials*, No. 47, Clarendon Press, Oxford, 1992, pp. 278–85.